Modeling and stability enhancement of a permanent magnet synchronous generator based DC system for More Electric Aircraft

Jiajun Yang, Hao Yan, Chunyang Gu, Shuo Wang, Weiduo Zhao, Patrick Wheeler, Giampaolo Buticchi

University of Nottingham
UK | CHINA | MALAYSIA

University of Nottingham Ningbo China, 199 Taikang East Road, Ningbo, 315100, Zhejiang, China.

First published 2021

This work is made available under the terms of the Creative Commons Attribution 4.0 International License:
http://creativecommons.org/licenses/by/4.0

The work is licenced to the University of Nottingham Ningbo China under the Global University Publication Licence:
https://www.nottingham.edu.cn/en/library/documents/research/global-university-publications-licence-2.0.pdf

University of Nottingham
UK | CHINA | MALAYSIA

Modeling and Stability Enhancement of a Permanent Magnet Synchronous Generator Based DC System for More Electric Aircraft

Jiajun Yang, *Student Member, IEEE*, Hao Yan, *Member, IEEE*, Chunyang Gu, *Member, IEEE*, Shuo Wang, *Member, IEEE*, Weiduo Zhao, *Member, IEEE*, Pat Wheeler, *Fellow, IEEE* and Giampaolo Buticchi, *Senior Member, IEEE*

***Abstract*—The concept of the More Electric Aircraft (MEA) is aimed at electrifying the mechanical, hydraulic, and pneumatic subsystems on aircraft. With increasing usage of power electronics, the architecture of on-board electrical power distribution systems (EPDS) becomes more complicated. Therefore, it is necessary to analyze the stability of the system. This paper firstly presents and validates an impedance model of a permanent magnet synchronous generator (PMSG) as a source and dual active bridge (DAB) converter as a load. These models are used for the stability analysis of a simple DC power system. In addition, two new control strategies are proposed to enhance the stability of the system. The stabilization effects of the new control strategies are verified with experimental results.**

***Index Terms*—DC microgrid, more electric aircraft, impedance, stability analysis, permanent magnet synchronous generator, dual active bridge converter.**

I. Introduction

To cope with the finite nature of energy resources, the concept of the more electric aircraft (MEA) has been proposed, aimed at electrifying on-board subsystems which currently utilize hydraulic, pneumatic, and mechanical power. These replacements benefit the aircraft with lower weight, lower environmental impact, and lower maintenance cost [1], [2]. Lately, significant progress on the electrification of the aircraft subsystems has been achieved. For example, a bleedless architecture is adopted for Boeing 787 which replaces the pneumatic subsystems with electrical subsystems. This scheme allows to electrically support the environmental control system and wing ice protection with lower fuel consumption and higher efficiency [3].

As the number of on-board electrical devices increases, it is inevitable that the demands of electrical power increase. Since the aircraft can be regarded as an isolated system with generators and loads, the on-board electrical power distribution system (EPDS) can be considered as a microgrid [4]. The expected characteristics of such on-board microgrids have been regulated in the standards such as MIL-STD-704F [5]. Compared to AC microgrids, DC microgrids have advantages of fewer conversion stages, lower bus current ratings, and lower power losses [6].

Fig. 1 shows a potential structure of DC microgrid for future MEA, where 540V HVDC buses are adopted for the increasing power [3]. The DC-DC converters are mainly used for creating different DC voltage levels to meet the requirement of loads and to provide galvanic isolation. In the family of DC-DC converters featuring galvanic isolation, the dual active bridge (DAB) converter is one of the most popular topologies due to its high power density, high efficiency, low device and component stresses, low switching losses and bidirectional power flow [7].

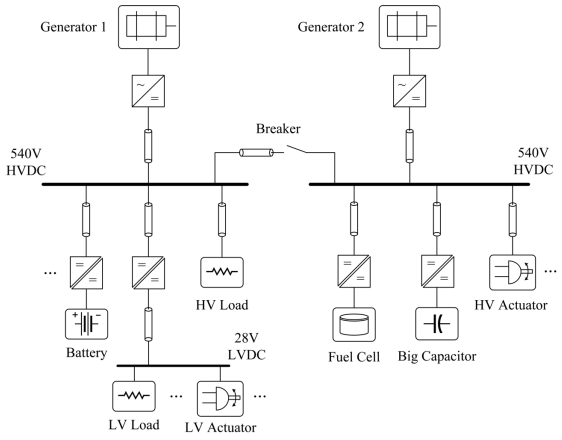

Fig. 1. A potential structure of DC microgrid for future MEA

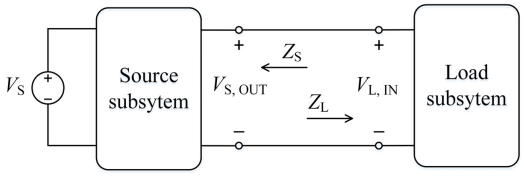

Fig. 2. Impedance model of a single bus DC system

With so many power electronic converters installed in the on-board EPS, the stability of the whole system becomes a concern since the power electronic converters could behave as a constant power load (CPL) and destabilize the system [8]. Hence, stability analysis of the whole system is necessary. To analyze the system stability, one of mainstream approaches is focused on the interaction between the impedance of source and load. Fig. 2 shows brief impedance model of a single-bus cascaded DC system formed with a source subsystem and a load subsystem. With a voltage source, the minor loop gain G_{MLG} is defined as the ratio of the source impedance Z_{S} to

the load impedance Z_{L}. On the premise of that the subsystems are individually stable, the stability of whole system can be ensured by checking if the Nyquist contour of G_{MLG} does not encircle (-1, 0), i.e. the Nyquist Criterion [9]. Based on that, several impedance-based criteria have been proposed. The most conservative is the Middlebrook Criterion [10]. The constraint boundary is given as

$$|G_{\mathrm{MLG}}| = |\frac{Z_{\mathrm{S}}}{Z_{\mathrm{L}}}| < \frac{1}{GM} \quad (GM > 1) \tag{1.1}$$

where GM is the desired gain margin. In addition to guaranteeing the system stability, the Middlebrook Criterion also takes care of the dynamics of converter itself and is not influenced by the input filter. However, it could lead to overdesign and make the components of input filter large. To loose the constraint boundary, the Gain Margin Phase Margin (GMPM) Criterion has been proposed [11], which is more moderate to the system design by giving additional phase margin if gain margin is not applicable. The constraint boundary of GMPM Criterion is given by:

$$|G_{\mathrm{MLG}}| < \frac{1}{GM}, \text{ if not}, |\angle G_{\mathrm{MLG}}| \leq 180^{\circ} - PM \tag{1.2}$$

where GM is the desired gain margin and PM is the desired phase margin. By liberating the phase margin, the system design becomes more flexible, although the phase information of subsystems is needed. Furthermore, the minor loop gain will be reciprocal if the source is a current source as presented in [12], given as

$$G_{\mathrm{MLG}} = \frac{Y_{\mathrm{S}}}{Y_{\mathrm{L}}} = \frac{Z_{\mathrm{L}}}{Z_{\mathrm{S}}} \tag{1.3}$$

So far, some works related to the impedance-based stability analysis have been presented by researchers. The harmonic instability problem of the traction network and multitrain has been investigated based on the impedance model in [13]. The stability of an AC microgrid is analyzed and enhanced by reshaping the source impedance in [14] and load impedance in [15]. The oscillation and resonance propagation problem between grid-connected converters in an AC microgrid is investigated based on impedance model, and therefore an active damper is proposed to dynamically reshape the source impedance for system stabilization in [16]. The stability analysis of a DC microgrid and its enhancement by virtual impedance is worked out in [17]. The stability analysis of a multi-generator single DC bus feeding a CPL has been carried out based on the impedance model in [18], where the source impedance is reshaped by proposing a dynamic droop controller. The stability criterion will change if the system structure becomes more complex. It is described in [19] that for a PV-battery hybrid power single-bus system the minor loop gain needs to be re-defined according to the control type of converters. Moreover, the definition of the minor loop gain can be generalized for hybrid power multi-bus systems [20].

Hence, it is always better to make the impedance model as accurate as possible to achieve the best possible prediction for system stability. This paper investigates the accurate impedance model of a permanent magnet synchronous generator (PMSG) as source and a DAB converter as load. The stability analysis of this system is presented. Besides, new control strategies are proposed to enhance the system stability. Section II presents the derivation process of the output impedance of PMSG and the input impedance of DAB converter. Section III validates the impedance model by Matlab and PLECS with feasible parameters. Section IV analyzes the system stability and enhances it by proposing two new control strategies. Section V shows the experimental results. In Section VI the work is summarized and conclusions are drawn.

II. Impedance Modeling

In this section, the output impedance of a PMSG and the input impedance of DAB converter are derived based on small signal equations at the operating point. Fig. 3 shows a basic control structure for the PMSG, where ω_{m} is the constant mechanical speed supported to PMSG, I_{d}, I_{q}, V_{d} and V_{q} are the d-q axis current and voltage, I_{o} is output current of three-phase rectifier, V_{dc} is DC bus voltage and C_{PMSG} is the output capacitor of PMSG. Correspondingly, the symbols annotated with '$*$' are references. Both voltage control and current control are implemented with PI controllers. The decoupling elements between d axis and q axis are omitted in the figure. To maximize the active power, the reference value of I_{d} is set to be zero. By defining the direction of d-q axis current is

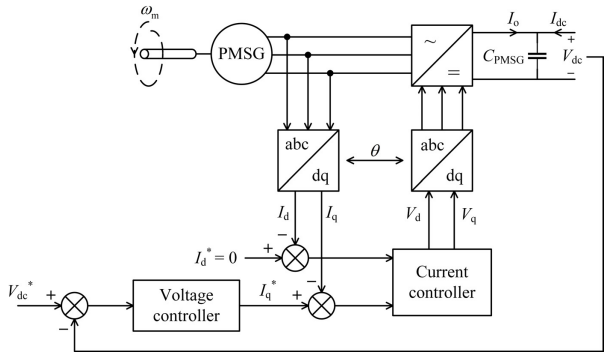

Fig. 3. A basic control structure of PMSG

positive if current goes out from PMSG, the machine equations in d-q frame are given as

$$\begin{cases} V_{\mathrm{d}} = -\left(R_{\mathrm{s}} + sL_{\mathrm{s}}\right) I_{\mathrm{d}} + \omega_{\mathrm{e}} L_{\mathrm{s}} I_{\mathrm{q}} \\ V_{\mathrm{q}} = -\left(R_{\mathrm{s}} + sL_{\mathrm{s}}\right) I_{\mathrm{q}} - \omega_{\mathrm{e}} L_{\mathrm{s}} I_{\mathrm{d}} + \omega_{\mathrm{e}} \psi_{\mathrm{PM}} \end{cases} \tag{2.1}$$

where R_{s} and L_{s} are the stator resistance and inductance, ω_{e} is the electrical speed equal to $p\omega_{\mathrm{m}}$ (p is the pole-pairs, ω_{m} is constant mechanical speed), ψ_{PM} is the flux linkage of the permanent magnet. Based on (2.1), the small signal equations can be derived as

$$\begin{cases} \hat{V}_{\mathrm{d}} = -\left(R_{\mathrm{s}} + sL_{\mathrm{s}}\right) \hat{I}_{\mathrm{d}} + \omega_{\mathrm{e}} L_{\mathrm{s}} \hat{I}_{\mathrm{q}} \\ \hat{V}_{\mathrm{q}} = -\left(R_{\mathrm{s}} + sL_{\mathrm{s}}\right) \hat{I}_{\mathrm{q}} - \omega_{\mathrm{e}} L_{\mathrm{s}} \hat{I}_{\mathrm{d}} \end{cases} \tag{2.2}$$

By applying a circuit averaging technique, the open loop model of PMSG can be obtained. Assuming that the d-q axes are perfectly decoupled, then only the components at q-axis

need to be considered. The control equations of q-axis can be given as

$$\begin{cases} \hat{I}_{\mathrm{q}}^{*} = \left(\hat{V}_{\mathrm{dc}}^{*} - \hat{V}_{\mathrm{dc}}\right) G_{\mathrm{v}}(s) \\ \left(\hat{I}_{\mathrm{q}}^{*} - \hat{I}_{\mathrm{q}}\right) G_{\mathrm{i}}(s) = \left(R_{\mathrm{s}} + sL_{\mathrm{s}}\right) \hat{I}_{\mathrm{q}} \end{cases} \tag{2.3}$$

where $G_{\mathrm{v}}(s)$ and $G_{\mathrm{i}}(s)$ are the transfer functions of voltage controller and current controller. The transferred power also accounts for the system dynamics. Since I_{d} is zero in steady state, and by applying the transformation with constant amplitude, the power equation of PMSG at steady state in ideal case can be given as

$$V_{\mathrm{dc}} I_{\mathrm{o}} = \frac{3}{2} V_{\mathrm{q}} I_{\mathrm{q}} \tag{2.4}$$

And the small signal equation of I_{o} can be derived as

$$\hat{I}_{\mathrm{o}} = \frac{1.5 I_{\mathrm{q}}}{V_{\mathrm{dc}}} \hat{V}_{\mathrm{q}} + \frac{1.5 V_{\mathrm{q}}}{V_{\mathrm{dc}}} \hat{I}_{\mathrm{q}} - \frac{I_{\mathrm{o}}}{V_{\mathrm{dc}}} \hat{V}_{\mathrm{dc}} \tag{2.5}$$

By combining (2.3) and (2.5), the closed loop transfer function block scheme of PMSG can be obtained as Fig. 4, where $G_{\mathrm{d,PMSG}}(s)$ is the first order delay function with time constant of a switching period. Hence, the output impedance of PMSG can be derived as (2.6). When it comes to the controller design of PMSG, the inner current controller should be designed to have larger bandwidth than the outer voltage controller. To facilitate the design, the current controller can be easily designed by cancelling the pole caused by stator impedance, and the voltage controller can be designed using the principle of 'symmetrical optimum' to maximize the phase margin [21]. The derivation process is omitted here. The transfer function of current controller is given as

$$G_{\mathrm{i}}(s) = k_{\mathrm{p,i}} + \frac{k_{\mathrm{i,i}}}{s} \tag{2.7}$$

where $k_{\mathrm{p,i}} = \omega_{\mathrm{BW,i}} L_{\mathrm{s}}$ and $k_{\mathrm{i,i}} = \omega_{\mathrm{BW,i}} R_{\mathrm{s}}$, then $\omega_{\mathrm{BW,i}}$ is the bandwidth of inner current loop. The transfer function of voltage controller is given as

$$G_{\mathrm{v}}(s) = k_{\mathrm{p,v}} + \frac{k_{\mathrm{i,v}}}{s} \tag{2.8}$$

where $k_{\mathrm{p,v}} = \frac{2C_{\mathrm{PMSG}} V_{\mathrm{dc}}}{3V_{\mathrm{q}}} \omega_{\mathrm{BW,v}} \sqrt{\frac{\omega_{\mathrm{BW,i}}}{\omega_{\mathrm{BW,v}}}}$ and $k_{\mathrm{i,v}} = \frac{2C_{\mathrm{PMSG}} V_{\mathrm{dc}}}{3V_{\mathrm{q}}} {\omega_{\mathrm{BW,v}}}^2 \sqrt{\frac{\omega_{\mathrm{BW,i}}}{\omega_{\mathrm{BW,v}}}}$, $\omega_{\mathrm{BW,v}}$ is the bandwidth of voltage controller. For a given phase margin θ, it exists

$$\frac{\omega_{\mathrm{BW,i}}}{\omega_{\mathrm{BW,v}}} = \left(\frac{1 + \cos\theta}{\sin\theta}\right)^2 \tag{2.9}$$

TABLE I
PARAMETERS OF PMSG

Symbol	Definition	Value
R_{s}	Stator resistance	4 mΩ
L_{s}	Stator inductance	40 μH
p	Number of pole pairs	1
f_{c}	Carrier (switching) frequency	20 kHz
$\omega_{\mathrm{BW,i}}$	Current controller bandwidth	1256.6 rad/s
V_{dc}	DC bus voltage	540 V
ω_{m}	Mechanical rotating speed	15000 rpm
ψ_{PM}	Flux linkage of the permanent magnet	0.127 Wb
C_{PMSG}	Output capacitor	10 mF
θ	Desired phase margin	60°

The input impedance of DAB converter including the input capacitor has been derived in [22] and shown as (2.10), where C_{i} and C_{o} are the input capacitance and output capacitance, $G_{\mathrm{v,DAB}}$ is the transfer function of voltage controller, R_{load} is the load resistance. The G_1, G_2, G_3 and G_4 are the small signal gains derived from power equation of DAB converter, given as

$$\begin{aligned} G_1 &= \frac{1}{2N f_{\mathrm{s}} L_{\mathrm{lk}}} \left(1 - |2d|\right) V_{\mathrm{o}}, G_2 = \frac{1}{2N f_{\mathrm{s}} L_{\mathrm{lk}}} (1 - |d|) d, \\ G_3 &= \frac{1}{2N f_{\mathrm{s}} L_{\mathrm{lk}}} \left(1 - |2d|\right) V_{\mathrm{i}}, G_4 = \frac{1}{2N f_{\mathrm{s}} L_{\mathrm{lk}}} (1 - |d|) d \end{aligned} \tag{2.11}$$

where N is the turn ratio of transformer, f_{s} is the switching frequency, L_{lk} is the leakage inductance, d is the phase shift ratio, V_{i} is the input voltage and V_{o} is the output voltage.

III. IMPEDANCE MODEL VALIDATION

In this section, the impedance model of the PMSG and the DAB converter is validated with the corresponding ideal switching model in PLECS. A set of feasible specifications are given in Table I and Table II.

1) Validation of the output impedance model of the PMSG: an ideal current source containing DC current and AC sinusoidal current is set as load to the output of switching model of PMSG. By observing the output voltage and current of the PMSG, the output impedance of PMSG at specific frequency can be calculated. Fig. 5 shows the output impedance of PMSG

$$Z_{\mathrm{o,PMSG}} = \frac{V_{\mathrm{dc}} \left[G_{\mathrm{i}}(s) + R_{\mathrm{s}} + sL_{\mathrm{s}}\right]}{sC_{\mathrm{PMSG}} V_{\mathrm{dc}} \left[G_{\mathrm{i}}(s) + R_{\mathrm{s}} + sL_{\mathrm{s}}\right] + G_{\mathrm{v}}(s) G_{\mathrm{i}}(s) \left[1.5V_{\mathrm{q}} - (R_{\mathrm{s}} + sL_{\mathrm{s}}) 1.5 I_{\mathrm{q}}\right] G_{\mathrm{d,PMSG}}(s) + I_{\mathrm{o}} \left[G_{\mathrm{i}}(s) + R_{\mathrm{s}} + sL_{\mathrm{s}}\right] G_{\mathrm{d,PMSG}}(s)} \tag{2.6}$$

$$Z_{\mathrm{i,DAB}} = \frac{G_3 G_{\mathrm{v,DAB}} R_{\mathrm{load}} + sC_{\mathrm{o}} R_{\mathrm{load}} + 1}{G_4 R_{\mathrm{load}} (G_2 - G_1 G_{\mathrm{v,DAB}}) + sC_{\mathrm{i}} (G_3 G_{\mathrm{v,DAB}} R_{\mathrm{load}} + sC_{\mathrm{o}} R_{\mathrm{load}} + 1)} \tag{2.10}$$

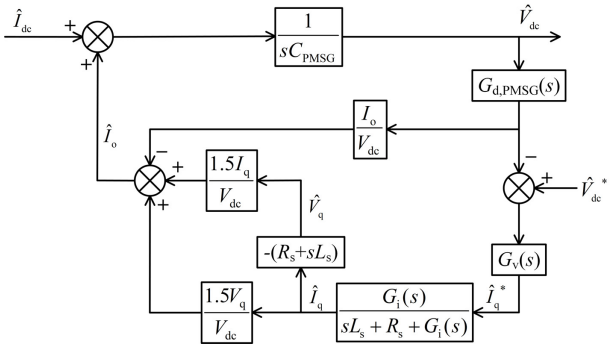

Fig. 4. Closed loop transfer function block scheme of PMSG

TABLE II
PARAMETERS OF DAB CONVERTER

Symbol	Definition	Value
V_{i}	Input voltage	540 V
V_{o}	Output voltage	270 V
N	Turn ratio of transformer	270/540
L_{lk}	Leakage inductance	10 μH
f_{s}	Switching frequency	50 kHz
$k_{\mathrm{p,DAB}}$	Proportional coefficient	0.02
$k_{\mathrm{i,DAB}}$	Integral coefficient	1
C_{i}	Input capacitor	6 mF
C_{o}	Output capacitor	6 mF

with output power of 500 kW. It can be observed that the proposed model is consistent with simulation measurements.

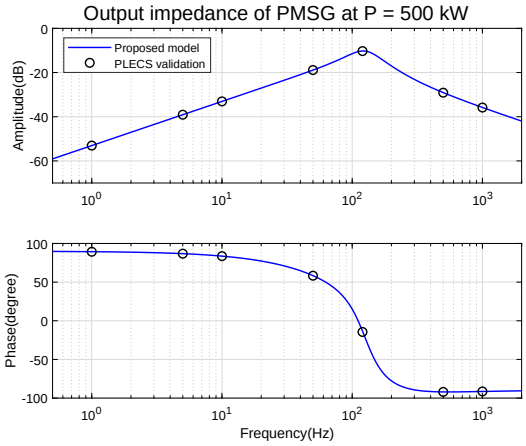

Fig. 5. The output impedance of PMSG with power of 500 kW

2) Validation of the input impedance model of DAB converter: an ideal voltage source containing DC voltage and AC sinusoidal voltage as small signal is set as source to the input of switching model of DAB converter. By observing the input voltage and the current goes into the DAB converter, the input impedance of DAB converter at specific frequency can be calculated. Fig. 6 shows the input impedance of DAB converter with input power of 50 kW. It can be seen that the proposed model is consistent with the simulation results.

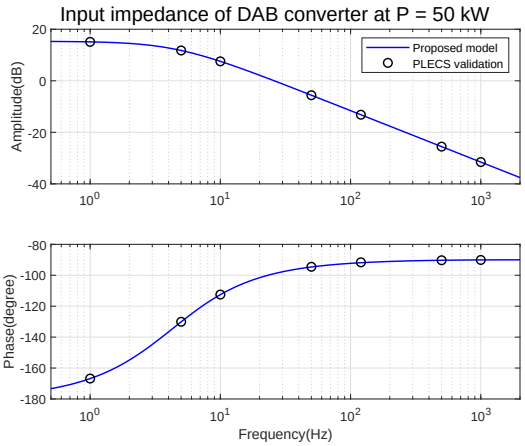

Fig. 6. The input impedance of DAB converter with power of 50 kW

TABLE III
PARAMETERS OF DC BUS CABLE

Symbol	Definition	Value
R_{wire}	Resistance of wire	3.3 mΩ
L_{wire}	Inductance of wire	21.2 μH

IV. STABILITY ANALYSIS OF A DC SYSTEM CONSISTING OF A PMSG AND A DAB CONVERTER

In this section, the stability system consisting of a PMSG, a DAB converter, and a controlled motor drive represented as a CPL, is analyzed by considering the impedance of DC bus cable. According to the electrical power capacity of Airbus A380, the rated power of system is set as 500 kW. Since the wingspan of A380 is almost 80 m, the maximum length of cable is assumed to be equal to 80 m if a PMSG is at one end and a DAB converter and a CPL are at another end of the wing; the DC bus cable is chosen to be a bunch of seven cables with type of ASNE0438-YV AWG 4/0 in [23], to handle the large current on DC bus. With the known diameter and length of each cable, the resistance and inductance of DC bus cable can be calculated using the formula in [24]. The parameters of DC bus cable are listed in TABLE III. Besides, considering the reality that the controlled motor drives take very large proportion of total on-board electrical power while the DC-DC converters only possess few, it is assumed that the CPL occupies 90% of system rated power and the DAB converter only occupies 10% in the following analysis.

Although the Nyquist Criterion provides the sufficient and necessary condition for system stability, it is discussed in [9] that different grouping of subsystems can influence how they will be designed. And different grouping of subsystems will also influence the accuracy of stability analysis based on bode diagram. Hence, to facilitate an accurate analysis of proposed control strategies subsequently, the PMSG, cable and input capacitor of DAB converter are grouped together to be the source impedance, the rest of DAB converter and the CPL are grouped to be the load impedance, shown in Fig. 7. It is noted that I_{p} is the current goes into the source subsystem.

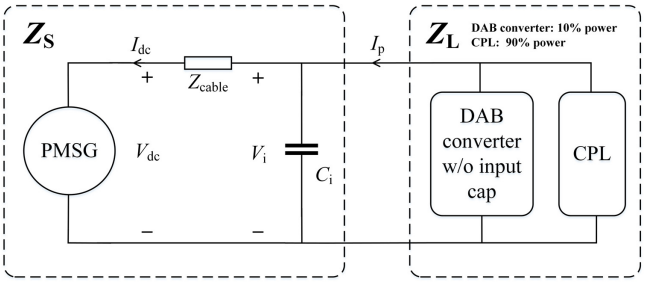

Fig. 7. Grouping details of subsystems

A. System instability

Fig. 8 shows the bode diagram of source impedance and load impedance at system power of 300 kW, 400 kW and 500 kW (in all cases the DAB converter keeps 50 kW) with original control (OC), i.e. PMSG controls the d-q current and its output voltage while DAB converter controls its output voltage only. It can be seen that the magnitude of Z_{S} and Z_{L} intersect at frequency of approximately 570 Hz when system power is 400 kW and 500 kW, indicating the system becomes unstable while a 570 Hz harmonic component appears in DC bus. Fig. 9 shows the Nyquist contour of minor loop gain G_{MLG} at system power of 300 kW, 400 kW and 500 kW. The Nyquist contour encircles (-1, 0) when system power is 400 kW and 500 kW, indicating the instability.

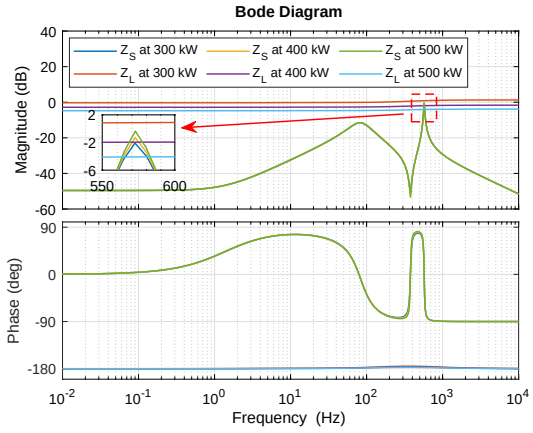

Fig. 8. Bode diagram: both source impedance and load impedance with OC, at 300 kW, 400 kW and 500 kW

B. Proposed control strategies for system stabilization

To deal with the system instability, two strategies 1) voltage sag pass-through control (VSPTC) and 2) point of load control (PLC) are proposed for the DAB converter and PMSG, respectively.

1) Method I: Voltage sag pass-through control (VSPTC): Compared to the original voltage control of a DAB converter, VSPTC links the input voltage and reference voltage by an extra high-pass filter. The transfer function block scheme with

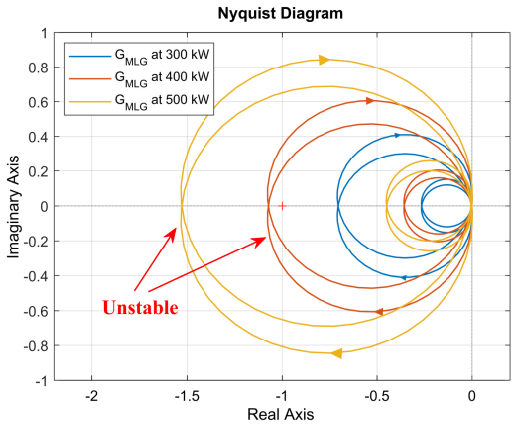

Fig. 9. Nyquist contour of G_{MLG} with OC, at 300 kW, 400 kW and 500 kW

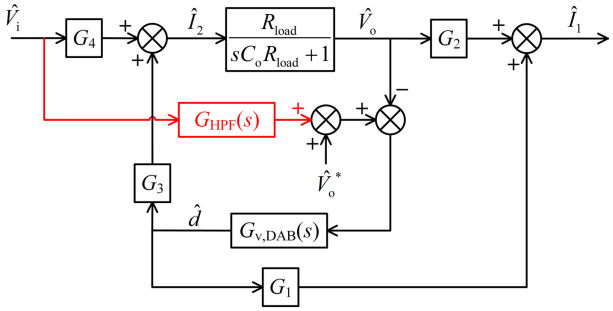

Fig. 10. The transfer function block scheme with VSPTC

VSPTC is shown in Fig. 10. The expression of high-pass filter is defined as

$$G_{\mathrm{HPF}}(s) = \frac{Ns}{s+\omega_{\mathrm{c}}} \tag{5.1}$$

where ω_{c} is the cut-off frequency. This feature of the DAB converter not only controls the load voltage, but also detects the variations in DC bus voltage and takes actions to counteract them. Fig. 11 shows the effect of VSPTC on Z_{L} with different cut-off frequency at system power of 500 kW. It can be seen that with the addition of high-pass filter the phase of Z_{L} at high frequencies is boosted. Moreover, the higher the cut-off frequency, the lower the magnitude and the less the phase boost at the intersection part. In this case, the cut-off frequency of the high-pass filter is set as 200 rad/s. Fig. 12 shows the source impedance with OC and load impedance with OC and VSPTC at system power of 500 kW. It can be seen that the phase around the intersection part is boosted, indicating a larger phase margin.

2) Method II: Point of load control (PLC): Point of load control means controlling the input voltage of load instead of the output voltage of source. If the PMSG controls its own output voltage, there will be a voltage drop on the cable, which will limit the power supplied to the load subsystem. If the PMSG controls the input voltage of the load subsystem, then the voltage drop on the cable can be compensated, resulting in a lower magnitude of source impedance. Since the loads

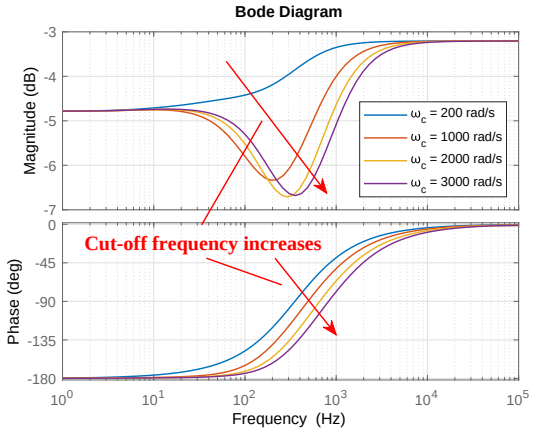

Fig. 11. The effect of VSPTC on Z_{L} with different cut-off frequency at system power of 500 kW

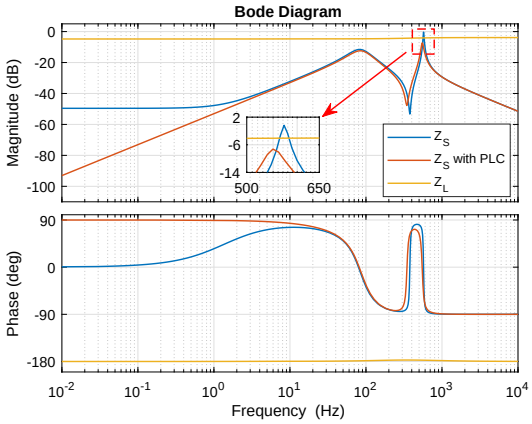

Fig. 14. Bode diagram: source impedance with OC and PLC, load impedance with OC, at 500 kW

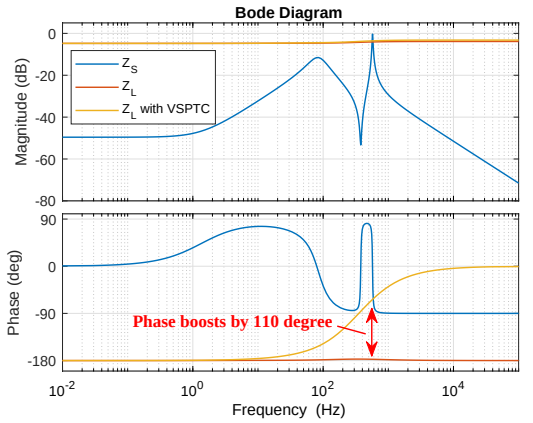

Fig. 12. Bode diagram: source impedance with OC, load impedance with OC and VSPTC, at 500 kW

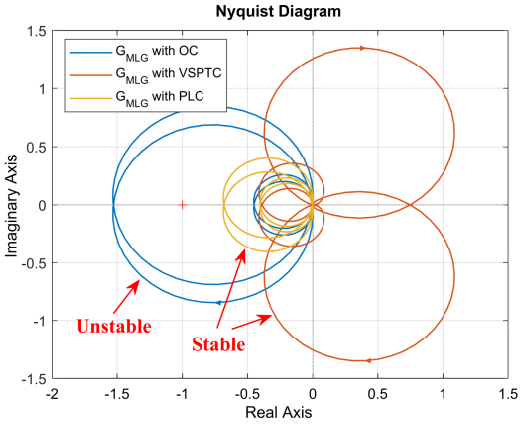

Fig. 15. The Nyquist contour of G_{MLG} with OC, VSPTC and PLC, at 500 kW

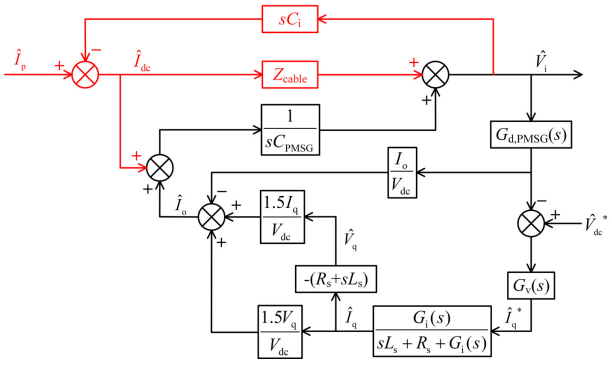

Fig. 13. The transfer function block scheme with PLC

could be far away from the sources in an on-board DC microgrid, the communication between the load sensor and source converter controller becomes a problem. To solve this problem, one of possible approaches is using broadband power line communication technique to achieve data transmission on DC bus, which features shorter communication links, lower noise levels, lower latency times and higher potential data rates [25]. In this case, it is assumed that the load voltage can be obtained by broadband power line communication. The communication delay up to 100 μs has no effect on the stability of the system, for longer delays that may be introduced by the communication system, the effects should be modeled and an appropriate reduction of the voltage controller bandwidth of PMSG is envisaged. Fig. 13 shows the transfer function block scheme with PLC. Fig. 14 shows the source impedance with OC and PLC and load impedance with OC at system power of 500 kW. It can be seen that with PLC the amplitude of source impedance is reduced at low frequencies, increasing the gain margin. As a trade-off, the phase of the source impedance at low frequencies is boosted, sacrificing the phase margin. In addition, it can be seen that with PLC the peak of source impedance around 570 Hz is diminished to avoid intersection with load impedance.

Fig. 15 shows the Nyquist contour of G_{MLG} with OC, VSPTC and PLC at 500 kW. It can be seen that both VSPTC and PLC can stabilize the system at 500 kW. Fig. 16 presents the simulation results of switching model with three control strategies in PLECS where the DAB converter keeps 50 kW

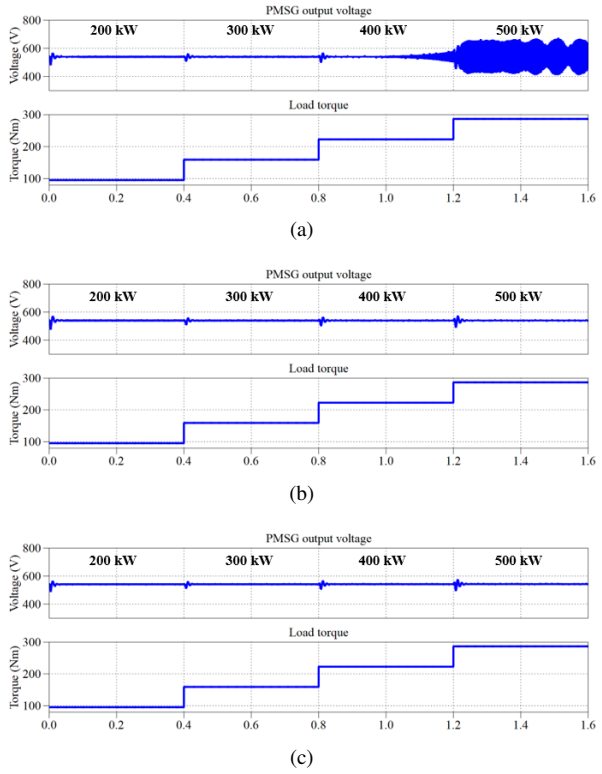

Fig. 16. Simulation waveform: Output voltage of PMSG and load torque of controlled motor drive when applying (a) OC, (b) VSPTC and (c) PLC as power increases 100 kW per 0.4 s

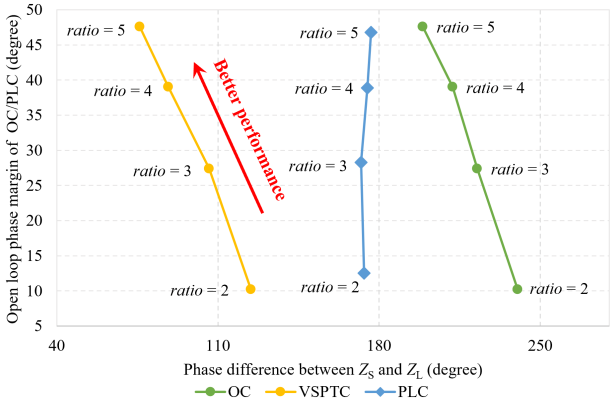

Fig. 17. Evaluation of three control strategies

and the controlled motor drive increases power by 100 kW, showing a good match with Fig. 15.

C. Evaluation of three control strategies

Although it is still possible to make system stable by tuning the control parameters, it would normally result in slower transients. To better highlight this trade-off, a Pareto plot of the opposing control goals (i.e. open loop phase margin of OC/PLC and phase difference between Z_S and Z_L on the critical frequency) is performed at system power of 500 kW, in which the ratio $\frac{\omega_{BW,i}}{\omega_{BW,v}}$ is changed with fixed $\omega_{BW,i}$. Fig. 17 shows the Pareto plot of evaluation. It needs to be noted

TABLE IV
EXPERIMENTAL PARAMETERS OF PMSG

Symbol	Definition	Value
R_s	Stator resistance	1 Ω
L_s	Stator inductance	0.72 mH
p	Number of pole pairs	21
f_c	Carrier (switching) frequency	20 kHz
V_{dc}	DC bus voltage	50 V
$k_{p,i}$	Proportional coefficient of current controller	2
$k_{i,i}$	Integral coefficient of current controller	2000
$k_{p,v}$	Proportional coefficient of voltage controller	2
$k_{i,v}$	Integral coefficient of voltage controller	500
ω_m	Mechanical rotating speed	500 rpm
ψ_{PM}	Flux linkage of the permanent magnet	0.021 Wb
C_{PMSG}	Output capacitor	0.34 mF

that the phase difference is measured at the most challenging point. To be more specific: For the cases in which Z_S and Z_L have intersections, the phase difference is measured at the point with the largest phase difference when the gain margin cannot be provided, marked as 'dot'; For the cases in which Z_S and Z_L have no intersections, the phase difference is measured at the point with the smallest gain margin, marked as 'diamond'. It can be seen from Fig. 17 that the phase difference between Z_S and Z_L is obviously diminished by applying the VSPTC, indicating the system stability is enhanced, and the intersection of magnitude of Z_S and Z_L is avoided by applying the PLC. Moreover, it shows that the open loop phase margin of OC/PLC increases as the $\omega_{BW,v}$ reduces, enhancing the stability of source subsystem itself.

V. EXPERIMENTAL RESULTS

In this section, the experimental setup and its parameters are given. The experimental results of the three control strategies mentioned above are presented under the prediction for system stability based on the proposed models. The experimental setup consists of a PMSG and a DAB converter, shown in Fig. 18. In (a), a multi three-phase machine is used as single three-phase mode by modifying the connection of coils. In (b), the 3-phase inverter is working as rectifier controlled by PLECS RT-box. In (c), the DAB converter is controlled by MPC5643L microcontroller, and two windings of a 4-winding transformer are used to achieve power transmission and galvanic isolation between two H-Bridges. The experimental parameters for the PMSG, DAB converter and DC bus cable are given in TABLE IV, TABLE V and TABLE VI.

According to the experimental parameters, the prediction for the system stability based on proposed models is carried out firstly. During the prediction process, the cut-off frequency of VSPTC is set as 80 rad/s and the load resistance decreases from 60 Ω to 30 Ω by 15 Ω per 3 seconds. As a result, the Nyquist contour encircles (-1, 0) only when load resistance is 30 Ω with OC. Fig. 19 shows the waveforms of output voltage of PMSG and load current of DAB converter under different control strategies. It can be seen in (a) that with OC,

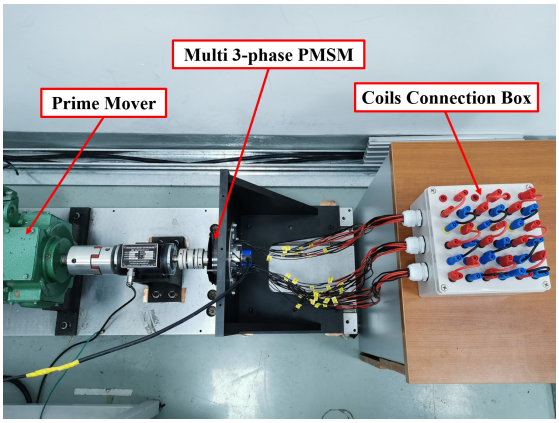

(a)

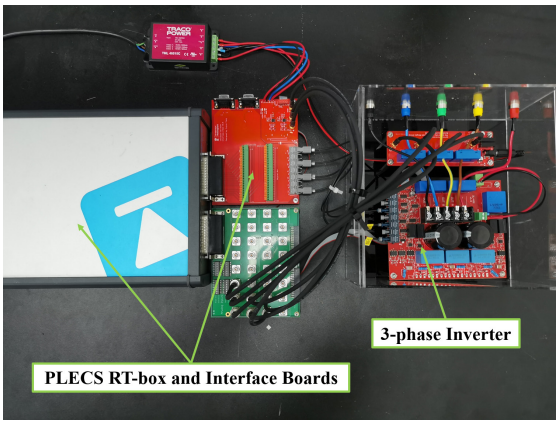

(b)

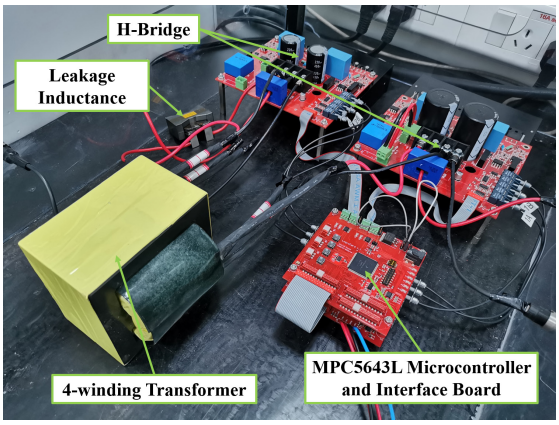

(c)

Fig. 18. Experimental setup: (a) test rig of PMSM, (b) 3-phase inverter and (c) DAB converter

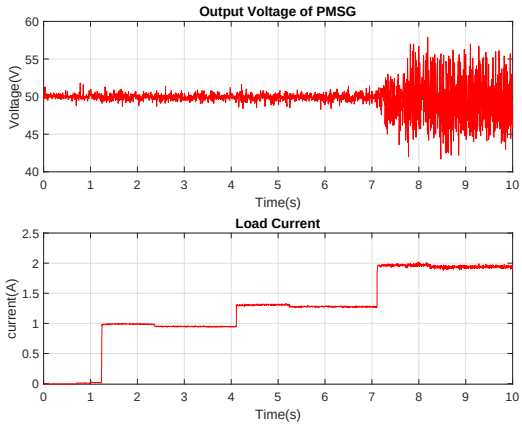

(a)

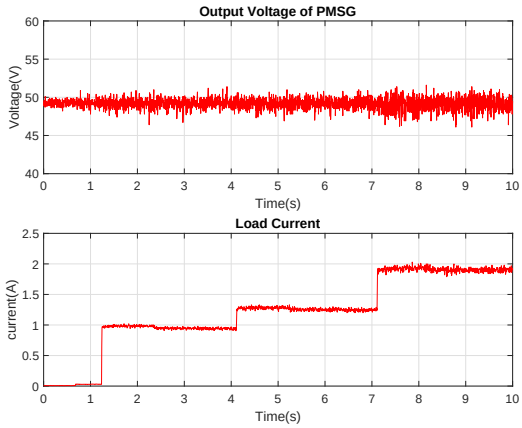

(b)

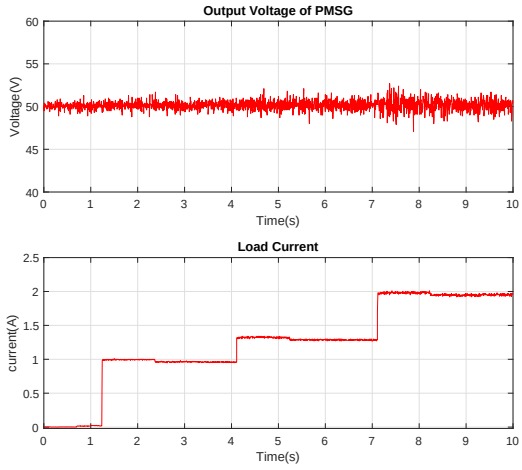

(c)

Fig. 19. Output voltage of PMSG and load current of DAB converter when applying (a) OC, (b) VSPTC and (c) PLC as load resistance decreases from 60 Ω to 30 Ω with step of 15 Ω per 3 seconds

the system becomes unstable when load resistance steps down from 45 Ω to 30 Ω, while (b) and (c) show that the system is still stable with VSPTC and PLC. This proves that both the VSPTC and PLC have postive effects on system stabilization.

VI. Conclusion

This paper proposes and validates the impedance model of PMSG and DAB converter. With the proposed models and considering the impedance of DC bus cable, the stability of a DC system including a PMSG and a DAB converter is analyzed. Since the impedance of DC bus cable could deteriorate the system stability, to solve this problem, two new control strategies named VSPTC and PLC are proposed,

TABLE V
EXPERIMENTAL PARAMETERS OF DAB CONVERTER

Symbol	Definition	Value
V_{i}	Input voltage	50 V
V_{o}	Output voltage	60 V
N	Turn ratio of transformer	270/270
L_{lk}	Leakage inductance	20 μH
f_{s}	Switching frequency	50 kHz
$k_{\mathrm{p,DAB}}$	Proportional coefficient	0.2
$k_{\mathrm{i,DAB}}$	Integral coefficient	10
C_{i}	Input capacitor	0.11 mF
C_{o}	Output capacitor	0.34 mF

TABLE VI
EXPERIMENTAL PARAMETERS OF DC BUS CABLE

Symbol	Definition	Value
R_{wire}	Resistance of wire	0.08 Ω
L_{wire}	Inductance of wire	160 μH

aimed at stabilizing the bus voltage. The stabilization effects of VSPTC and PLC on system are verified by both simulation and experiment. In addition, with the impedance model, the stability analysis of systems with more complex structures can be carried out. Also, by considering both the impedance model and the proposed control strategies, the system can be designed and optimized for different cases.

REFERENCES

[1] J. A. Rosero, J. A. Ortega, E. Aldabas, and L. Romeral, "Moving towards a more electric aircraft," *IEEE Aerospace and Electronic Systems Magazine*, vol. 22, no. 3, pp. 3–9, March 2007.

[2] B. Sarlioglu and C. T. Morris, "More electric aircraft: Review, challenges, and opportunities for commercial transport aircraft," *IEEE Transactions on Transportation Electrification*, vol. 1, no. 1, pp. 54–64, 2015.

[3] V. Madonna, P. Giangrande, and M. Galea, "Electrical power generation in aircraft: Review, challenges, and opportunities," *IEEE Transactions on Transportation Electrification*, vol. 4, no. 3, pp. 646–659, 2018.

[4] G. Buticchi, S. Bozhko, M. Liserre, P. Wheeler, and K. Al-Haddad, "On-board microgrids for the more electric aircraft-technology review," *IEEE Transactions on Industrial Electronics*, vol. 66, no. 7, pp. 5588–5599, 2019.

[5] *MIL-STD-704F Aircraft Electric Power Characteristics*. Richmond, VA, USA: Dept. Defence, 2004.

[6] D. Salomonsson and A. Sannino, "Low-voltage dc distribution system for commercial power systems with sensitive electronic loads," *IEEE Transactions on Power Delivery*, vol. 22, no. 3, pp. 1620–1627, 2007.

[7] M. N. Kheraluwala, R. W. Gascoigne, D. M. Divan, and E. D. Baumann, "Performance characterization of a high-power dual active bridge dc-to-dc converter," *IEEE Transactions on Industry Applications*, vol. 28, no. 6, pp. 1294–1301, 1992.

[8] A. Emadi, A. Khaligh, C. H. Rivetta, and G. A. Williamson, "Constant power loads and negative impedance instability in automotive systems: definition, modeling, stability, and control of power electronic converters and motor drives," *IEEE Transactions on Vehicular Technology*, vol. 55, no. 4, pp. 1112–1125, 2006.

[9] S. D. Sudhoff, S. F. Glover, P. T. Lamm, D. H. Schmucker, and D. E. Delisle, "Admittance space stability analysis of power electronic systems," *IEEE Transactions on Aerospace and Electronic Systems*, vol. 36, no. 3, pp. 965–973, 2000.

[10] R. D. Middlebrook, "Input filter considerations in design and application of switching regulators," in *Conf. Rec. IEEE IAS Annu. Meeting*, 1976, pp. 366–382.

[11] C. M. Wildrick, F. C. Lee, B. H. Cho, and B. Choi, "A method of defining the load impedance specification for a stable distributed power system," *IEEE Transactions on Power Electronics*, vol. 10, no. 3, pp. 280–285, 1995.

[12] J. Sun, "Impedance-based stability criterion for grid-connected inverters," *IEEE Transactions on Power Electronics*, vol. 26, no. 11, pp. 3075–3078, 2011.

[13] H. Tao, H. Hu, X. Wang, F. Blaabjerg, and Z. He, "Impedance-based harmonic instability assessment in a multiple electric trains and traction network interaction system," *IEEE Transactions on Industry Applications*, vol. 54, no. 5, pp. 5083–5096, 2018.

[14] A. A. A. Radwan and Y. A. I. Mohamed, "Modeling, analysis, and stabilization of converter-fed ac microgrids with high penetration of converter-interfaced loads," *IEEE Transactions on Smart Grid*, vol. 3, no. 3, pp. 1213–1225, 2012.

[15] ——, "Analysis and active-impedance-based stabilization of voltage-source-rectifier loads in grid-connected and isolated microgrid applications," *IEEE Transactions on Sustainable Energy*, vol. 4, no. 3, pp. 563–576, 2013.

[16] X. Wang, F. Blaabjerg, M. Liserre, Z. Chen, J. He, and Y. Li, "An active damper for stabilizing power-electronics-based ac systems," *IEEE Transactions on Power Electronics*, vol. 29, no. 7, pp. 3318–3329, 2014.

[17] X. Lu, K. Sun, J. M. Guerrero, J. C. Vasquez, L. Huang, and J. Wang, "Stability enhancement based on virtual impedance for dc microgrids with constant power loads," *IEEE Transactions on Smart Grid*, vol. 6, no. 6, pp. 2770–2783, 2015.

[18] F. Gao and S. Bozhko, "Modeling and impedance analysis of a single dc bus-based multiple-source multiple-load electrical power system," *IEEE Transactions on Transportation Electrification*, vol. 2, no. 3, pp. 335–346, 2016.

[19] X. Zhang, X. Ruan, and C. K. Tse, "Impedance-based local stability criterion for dc distributed power systems," *IEEE Transactions on Circuits and Systems I: Regular Papers*, vol. 62, no. 3, pp. 916–925, 2015.

[20] P. Pan, W. Chen, L. Shu, H. Mu, K. Zhang, M. Zhu, and F. Deng, "An impedance-based stability assessment methodology for dc distribution power system with multivoltage levels," *IEEE Transactions on Power Electronics*, vol. 35, no. 4, pp. 4033–4047, 2020.

[21] R. Teodorescu, M. Liserre, and P. Rodriguez, *Grid Converters for Photovoltaic and Wind Power Systems*. West Sussex, UK: John Wiley & Sons, 2011.

[22] J. Yang, G. Buticchi, H. Yan, C. Gu, H. Zhang, and P. Wheeler, "Impedance-based sensitivity analysis of dual active bridge dc-dc converter," in *2019 IEEE 13th International Conference on Compatibility, Power Electronics and Power Engineering (CPE-POWERENG)*, 2019, pp. 1–5.

[23] Nexans, *Aircraft Wires and Cables*, 2007.

[24] F. W. Grover, *Inductance Calculations: Working Formulas and Tables. Courier Corporation*, 2004.

[25] S. Dominiak, S. Serbu, S. Schneele, F. Nuscheler, and T. Mayer, "The application of commercial power line communications technology for avionics systems," in *2012 IEEE/AIAA 31st Digital Avionics Systems Conference (DASC)*, 2012, pp. 7E1–1–7E1–14.

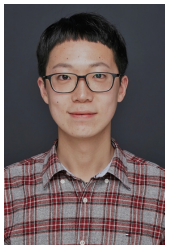

Jiajun Yang (Student Member, IEEE) received the B.Eng. degree (Hons.) in electrical and electronic engineering in 2017, from the University of Nottingham Ningbo China, Ningbo, China, where he is currently working toward the Ph.D. degree with the Key Laboratory of More Electric Aircraft Technology of Zhejiang Province.

From 2017 to 2018, he was a hardware engineer with the Nottingham Electrification Centre. His current research interests include high power density dc-dc converters and stability analysis of dc microgrids for the more electric aircraft.

Hao Yan (Member, IEEE) received the B.S., M.S. and Ph.D. degrees in electrical engineering from the Harbin Institute of Technology, Harbin, China, in 2011, 2013 and 2018, respectively.

From 2017 to 2019, he joined the Power Electronics, Machines and Control Group, University of Nottingham, Ningbo, China, and worked on power electronics for electrical drives for two years. From 2019 to 2020, he was a Research Fellow with the Rolls-Royce @ NTU Corporate Lab, Nanyang Technological University, Singapore 639798. He is currently an Associate Professor with the School of Civil Aviation, Northwestern Polytechnical University, Xi'an, China. His current research interests include permanent-magnet machine drives and power converters in More Electric Aircraft.

Chunyang Gu (Member, IEEE) was born in Heilongjiang, China, in 1988. She received BSc degree from Harbin Institute of Technology, Harbin, China, in 2010, and PhD degree from Tsinghua University, Beijing, China, in 2015, both in electrical engineering.

In 2015, she went to the University of Nottingham, UK, where she was a postdoc research fellow in Power Electronics, Machines and Control (PEMC) Research Group. Since 2017, she has been an Assistant Professor in Department of Electrical and Electronic Engineering and PEMC Research Group, University of Nottingham Ningbo China. Her research interests include power electronics for transportation electrification, renewable energy and grid applications, e.g. solid-state transformer, solid-state circuit breaker, multi-level converter topologies and control, application of wide-band-gap semiconductor devices, power electronics in EV, railway, marine and MEA.

Shuo Wang (Member, IEEE) received the bachelor degree in automation from Hebei university of Technology in 2011, Tianjin, China, master degree in control science and engineering from Tianjin University in 2014, Tianjin, China, and Ph.D. degree in control science and engineering from Tongji University in 2019, Shanghai, China.

From 2017 to 2018, he became a Visiting researcher with Power Electronics, Machines and Control Group (PEMC Group), University of Nottingham, Nottingham, U.K. He is current working as a senior research fellow in university of Nottingham, Ningbo, China. His current research interests include high performance torque control, sensorless control and flux-weakening control used for permanent magnet synchronous machines, synchronous reluctance machines and permanent magnet-assisted synchronous reluctance machines.

Weiduo Zhao (Member, IEEE) was born in Harbin, China, in 1985. He received the bachelor's degree in electrical engineering from the Taiyuan University of Technology, Taiyuan, China, in 2008, and the M.Sc. degree and Ph.D degree in electrical engineering from the Harbin Institute of Technology, Harbin, China, in 2010 and 2015, respectively.

He is currently a senior research fellow with the Power Electronics, Machines and Control Group, The University of Nottingham, Ningbo, China. His research interests include high-performance electric machines and drives, pulsed power systems, and thermal management.

Dr. Zhao was a recipient of the Peter J. Kemmey Memorial Scholarship from the 17th International Electromagnetic Launch Symposium, San Diego, CA, USA, in 2014.

Pat Wheeler (Fellow, IEEE) received his BEng [Hons] degree in 1990 from the University of Bristol, UK. He received his PhD degree in Electrical Engineering for his work on Matrix Converters from the University of Bristol, UK in 1994. In 1993 he moved to the University of Nottingham and worked as a research assistant in the Department of Electrical and Electronic Engineering. In 1996 he became a Lecturer in the Power Electronics, Machines and Control Group at the University of Nottingham, UK. Since January 2008 he has been a Full Professor in the same research group.

He was Head of the Department of Electrical and Electronic Engineering at the University of Nottingham from 2015 to 2018. He is currently the Head of the Power Electronics, Machines and Control Research Group, Global Director of the University of Nottinghamâs Institute of Aerosapce Technology and was the Li Dak Sum Chair Professor in Electrical and Aerospace Engineering. He is a member of the IEEE PELs AdCom and is currently an IEEE PELS Vice-President. He has published over 750 academic publications in leading international conferences and journals.

Giampaolo Buticchi (Senior Member, IEEE) received the Master degree in Electronic Engineering in 2009 and the Ph.D degree in Information Technologies in 2013 from the University of Parma, Italy. In 2012 he was visiting researcher at The University of Nottingham, UK. Between 2014 and 2017, he was a post-doctoral researcher, and Guest Professor at the University of Kiel, Germany. During his stay in Germany, he was awarded with the Von Humboldt Postdoctoral Fellowship to carry out research related to fault tolerant topologies of smart transformers.

In 2017 he was appointed as Associate Professor in Electrical Engineering at The University of Nottingham Ningbo China and as Head of Power Electronics of the Nottingham Electrification Center. He was promoted to Professor in 2020. His research focuses on power electronics for renewable energy systems, smart transformer fed micro-grids and dc grids for the More Electric Aircraft. Dr. Buticchi is one of the advocates for DC distribution systems and multi-port power electronics onboard the future aircraft.

He is author/co-author of more than 230 scientific papers, an Associate Editor of the IEEE Transactions on Industrial Electronics, the IEEE Transactions on Transportation Electrification and the IEEE Open Journal of the Industrial Electronics Society. He is currently the Chair of the IEEE-IES Technical Committee on Renewable Energy Systems and the IES Energy Cluster Delegate.